

Dispersive interactions between standard and Dirac materials and the role of dimensionality

Dai-Nam Le^{1,2,3}, Pablo Rodriguez-Lopez⁴, Lilia M. Woods^{1,5}

¹Department of Physics, University of South Florida, Tampa, Florida 33620, USA

²Atomic Molecular and Optical Physics Research Group, Advanced Institute of Materials Science, Ton Duc Thang University, Ho Chi Minh City 700000, Vietnam

³Faculty of Applied Sciences, Ton Duc Thang University, Ho Chi Minh City 700000, Vietnam

⁴Área de Electromagnetismo and Grupo Interdisciplinar de Sistemas Complejos (GISC), Universidad Rey Juan Carlos, 28933, Móstoles, Madrid, Spain

⁵Author to whom all correspondence should be addressed

E-mail: ledainam@tdtu.edu.vn (Dai-Nam Le)

E-mail: pablo.ropez@urjc.es (Pablo Rodriguez-Lopez)

E-mail: lmwoods@usf.edu (Lilia M. Woods)

Abstract. The van der Waals interaction plays a prominent role between neutral objects at separations where short ranged chemical forces are negligible. This type of dispersive coupling is determined by the interplay between geometry and response properties of the materials making up the objects. Here, we investigate the van der Waals interaction between 1D, 2D, and 3D standard and Dirac materials within the Random Phase Approximation, which takes into account collective excitations originating from the electronic Coulomb potential. A comprehensive understanding of characteristic functionalities and scaling laws are obtained for systems with parabolic energy dispersion (standard materials) and crossing linear bands (Dirac materials). By comparing the quantum mechanical and thermal limits the onset of thermal fluctuations in the van der Waals interaction is discussed showing that thermal effects are significantly pronounced at smaller scales in reduced dimensions.

Submitted to: *Journal of Physics: Materials*

1. Introduction

The exchange of electromagnetic excitations of two objects brought together results in a dispersive ubiquitous force whose sign and magnitude depend on the materials properties and geometry [1, 2]. At short separations, this exchange is instantaneous and the interaction is termed as the van der Waals (vdW) force whose main contribution comes from exponentially decaying surface modes. The vdW interaction is important for the stability of layered materials and composites made of chemically inert components. It also plays a significant role in the organization and complex behavior of biological systems, including lipids, membranes, and proteins.

In the simplest possible way, pair-wise summation of interatomic Lennard-Jones type of potentials may be used to estimate the vdW interaction between molecules and/or between extended objects [3, 4]. However, such a simplified approach does not take into account collective effects, which become significant for nondilute systems. By placing objects close to each other, their density fluctuations become affected by the mutual Coulomb interaction, which can result in different behavior of the vdW force when compared with results obtained by the pairwise summation method [5]. To capture electron correlation effects in the response properties of the interacting materials as well as their vdW force one can use the Random Phase Approximation (RPA), which is a second-order perturbative nonretarded approach with respect to the Coulomb interaction. This method has been successfully applied to a variety of systems [6, 7, 8, 9, 10]. Advanced computational techniques to calculate vdW interactions from first principles based on the RPA approach as well as other techniques have also been developed and shown to give accurate results in many weakly bound systems [11, 12, ?, ?, ?, ?].

Understanding how distinct properties of the materials affect the vdW interaction in different dimensions is particularly important in the context of many recent discoveries of topologically nontrivial systems [13, 14]. Given that the electronic structure and dimensionality determine the polarization properties of materials, it is important to investigate this interplay in the ubiquitous vdW force. Distinguishing between materials with parabolic and linear energy dispersions in one, two, and three dimensions can provide useful comprehensive insight in various asymptotic regimes of dis-

persive interactions involving standard and Dirac systems. Results from such investigations can also serve as a guide to interpret first principles simulations and experimental measurements for dispersive interactions for various systems.

In this paper, we utilize the RPA approach to calculate the density response function for 1D, 2D, and 3D materials with parabolic and linear energy dispersions. The vdW interaction is obtained based on the density-density correlator by treating the mutual Coulomb coupling as a perturbation [15]. By analyzing the characteristic behaviors in the dielectric response, we are able to provide a comprehensive description of the vdW interaction by elucidating the roles of electronic structure and dimensionality. By comparing the obtained results in the quantum mechanical and thermal limits, the onset of thermal fluctuations in the different dimensionalities is discussed. Unique features in terms of scaling laws and their dependence upon the Fermi level in the various dimensions are also obtained for standard and Dirac materials.

2. Dispersive Interactions - the RPA limit

The interacting objects in 1D, 2D, and 3D geometries are schematically shown in Fig. 1. In each case, the objects are placed in vacuum and are separated by a distance d along the z -axis. The wires in Fig. 1a are with diameters such that $w \ll d$ and the layers in Fig. 1b are assumed to be infinitely thin. The 3D objects in Fig. 1c are taken to be semi-infinite.

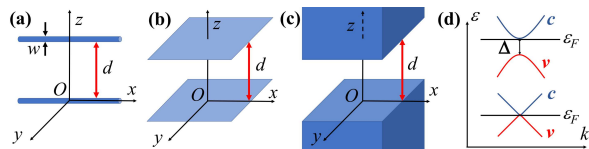


Figure 1. Schematics of two identical isotropic (a) 1D, (b) 2D, and (c) 3D materials in vacuum separated by a distance d along the z -axis. The 1D systems are taken as wires with a diameter $w \ll d$. The 2D layers are infinitely thin. (d) Schematics of the conduction (c) and valence (v) parabolic and crossing linear bands. A band gap Δ separates the c and v regions. The Fermi level is denoted as ε_F .

At smaller separations, the vdW dispersive force is determined by the instantaneous exchange by exponentially decaying modes localized on the surface of each object. These are p -polarized electromagnetic excitations and the interaction energy can be found as

a result of the Coulomb potential between the density fluctuations in the objects [15, 6],

$$F^{(N)} = \int \frac{d^N \mathbf{q}}{(2\pi)^N} \times \left. \frac{\partial \mathcal{V}^{(N)}(\mathbf{q}, z)}{\partial z} \right|_{z=d} \langle n_1(\mathbf{q}) n_2(-\mathbf{q}) \rangle^{(N)}. \quad (1)$$

In the above integral over the wave vector \mathbf{q} , N denotes the dimensionality and $\mathcal{V}^{(N)}$ is the Coulomb interaction between the objects. Also, $\langle n_1(\mathbf{q}) n_2(-\mathbf{q}) \rangle^{(N)}$ is the density-density correlator determined by the density fluctuations $n_1(\mathbf{q})$ and $n_2(-\mathbf{q})$ in the two objects (denoted as (1), (2)). The density-density correlator at finite temperature T in the RPA takes into account the collective screening effects and it is taken at imaginary Matsubara frequencies $\omega_l = 2\pi k_B T l / \hbar$ for the calculations of the vdW interaction [15, 6],

$$\begin{aligned} \langle n_1(\mathbf{q}) n_2(-\mathbf{q}) \rangle^{(N)} &= \\ &= k_B T \sum_{l=0}^{+\infty} \chi_1^{(N)}(\mathbf{q}, i\omega_l) \mathcal{W}(\mathbf{q}, d) \chi_2^{(N)}(\mathbf{q}, i\omega_l), \\ &= \frac{2k_B T}{\mathcal{V}^{(N)}(\mathbf{q}, d)} \sum_{l=0}^{+\infty} \left\{ \left[\frac{v_0^{(N)}(\mathbf{q})}{\mathcal{V}^{(N)}(\mathbf{q}, d)} \right]^2 \times \right. \\ &\quad \left. \times \left[1 - \frac{1}{v_0^{(N)}(\mathbf{q}) \chi_0^{(N)}(\mathbf{q}, i\omega_l)} \right]^2 - 1 \right\}^{-1}, \quad (2) \end{aligned}$$

where $v_0^{(N)}(\mathbf{q})$ is the Coulomb interaction of electrons inside each material in reciprocal \mathbf{q} space and $\chi_0^{(N)}(\mathbf{q}, \omega)$ is the bare polarization function. Within the RPA method, the screened Coulomb interaction $\mathcal{W}_0^{(N)}(\mathbf{q}, z) = \frac{\mathcal{V}_0^{(N)}(\mathbf{q}, z)}{1 - \chi_1^{(N)}(\mathbf{q}, i\omega_l) \mathcal{V}_0^{(N)}(\mathbf{q}, z) \chi_2^{(N)}(\mathbf{q}, i\omega_l)}$ and the screened polarization function $\chi_{1,2}^{(N)}(\mathbf{q}, i\omega_l) = \frac{\chi_0^{(N)}(\mathbf{q}, i\omega_l)}{1 - v_0^{(N)}(\mathbf{q}) \chi_0^{(N)}(\mathbf{q}, i\omega_l)}$ are obtained by summing connected bubble diagrams within the Feynman diagrammatic representation [15, 16, 17]. The prime in the summation indicates that the $l = 0$ term is multiplied by $1/2$.

It is apparent that for the interaction calculations, we need to distinguish the Coulomb coupling in each object and the Coulomb coupling between the objects. These can be derived from standard electrostatics following Gauss law (see Supplementary Information) and the results are summarized in Table 1 for the 1D, 2D and 3D cases from Fig. 1.

The polarization function $\chi_0^{(N)}(\mathbf{q}, \omega)$ corresponds to a single bubble diagram and it is given as [15, 16, 17]

$$\begin{aligned} \chi_0^{(N)}(\mathbf{q}, \omega) &= g \sum_{\mu, \nu} \int \frac{d^N \mathbf{k}}{(2\pi)^N} \mathcal{F}_{\nu, \mu}(\mathbf{k}, \mathbf{q}) \times \\ &\quad \times \frac{f(\varepsilon_\mu(\mathbf{k})) - f(\varepsilon_\nu(\mathbf{k} + \mathbf{q}))}{i\hbar\omega - [\varepsilon_\nu(\mathbf{k} + \mathbf{q}) - \varepsilon_\mu(\mathbf{k})]}, \quad (3) \end{aligned}$$

where g is the degeneracy of the electronic states, $\varepsilon_{\mu, \nu}$ are the eigenenergies of the underlying Hamiltonian of the specific material making up the objects, and $f(\varepsilon_{\mu, \nu})$ are the Fermi distribution functions. The factor $\mathcal{F}_{\nu, \mu}(\mathbf{k}, \mathbf{q}) = |\langle \nu, \mathbf{k} + \mathbf{q} | e^{i\mathbf{q} \cdot \mathbf{r}} | \mu, \mathbf{k} \rangle|^2 = |\langle u_{\nu, \mathbf{k} + \mathbf{q}} | u_{\mu, \mathbf{k}} \rangle|^2$ corresponds to the overlap integral between the Bloch eigenstates $|u_{\mu, \mathbf{k}}\rangle$ of the Hamiltonian.

Here we are interested in two types of systems: standard materials whose conduction (c) and valence (v) energy bands have a typical parabolic dispersion and Dirac materials characterized by crossing energy bands with a linear dispersion (schematics shown in Fig. 1d). For the considered systems, the energy dispersion and overlap integrals can be calculated in the long-wave length limit [16, 17, 18, 19] and the results are presented in Table 2. Note that the range of validity for the linear dispersion $\varepsilon_{c, v} = \pm \hbar v_F k$ is taken to be determined by a bandwidth ε_{max} . For standard materials, the parabolic conduction and valence bands are separated by a band gap Δ . One notes that when there is no band gap and the conduction and valence bands touch at a point at the Fermi level, the overlap integral is $\mathcal{F}_{\nu, \mu} = \delta_{\nu\mu}$. For Dirac materials, the overlap integral depends on the angle between the \mathbf{k}, \mathbf{q} wave vectors, $\theta_{\mathbf{k}, \mathbf{q}}$, as well as the ratio q^2/k^2 . Relevant details are given in the Supplementary Information.

Eq. Equation (3) captures interband and intraband transitions at imaginary frequency and the expressions from Table 2 allow explicit calculations for the bare polarization function for both types of materials in all dimensions. In addition to the general formulas for all materials and both types of transitions, analytical expressions for $\chi_0^{(N)}$ in the long wavelength approximation are shown in the Supplementary Information. Furthermore, the dependence of $\chi_0^{(N)}$ as a function of Matsubara frequencies scaled by the Fermi level is shown in Fig. 2 for some representative cases. We find that in standard materials, at small $\hbar\omega_l/\varepsilon_F$ the response function is dominated by intraband transitions, as expected. However, while in 2D the intraband contribution is almost a constant (essentially determined by the gap), in 3D the intraband part changes sign at very small $\hbar\omega_l/\varepsilon_F$. Our calculations also show (see Supplementary Information), that in 2D massless Dirac material a cancellation between the intra and interband contributions occurs at $\varepsilon_F \ll \hbar\omega$; as a result, doping is a dominant factor in the small imaginary frequency range.

In 3D Dirac materials, we find that the bandwidth specifying the validity of the linear band approximation for the energy dispersion, plays a prominent role. In fact, the interband contribution to χ_0 depends explicitly on ε_{max} . This is consistent with previous results for the interband components of the optical

Table 1. Coulomb coupling inside each object, $v_0^{(N)}(\mathbf{q})$, and between the objects, $\mathcal{V}^{(N)}(\mathbf{q}, z)$, where e is the electron charge, γ_E - Euler-Mascheroni number, w - width of the 1D object, $q_\perp = \sqrt{q_x^2 + q_y^2}$, and $K_0(y)$ - the modified Bessel function of second kind.

1D		2D	3D
$v_0^{(N)}(\mathbf{q})$	$v_0^{(1D)}(q_x) = 2e^2 \left[\ln \left(\frac{2}{ q_x w} \right) - \gamma_E \right]$	$v_0^{(2D)}(\mathbf{q}) = \frac{2\pi e^2}{q_\perp}$	$v_0^{(3D)}(\mathbf{q}) = \frac{4\pi e^2}{q^2}$
$\mathcal{V}^{(N)}(\mathbf{q}, z)$	$\mathcal{V}^{(1D)}(q_x, z) = 2e^2 K_0(q_x z)$	$\mathcal{V}^{(2D)}(\mathbf{q}, z) = \frac{2\pi e^2}{q_\perp} e^{-q_\perp z}$	$\mathcal{V}^{(3D)}(\mathbf{q}, z) = \frac{4\pi e^2}{q^2} e^{-q_\perp z}$

Table 2. Energy dispersion $\varepsilon_{c,v}(\mathbf{k})$ for the conduction (c) and valence (v) bands and corresponding overlap integral $\mathcal{F}_{\nu,\mu}(\mathbf{k}, \mathbf{q})$ for standard and Dirac materials in the long-wavelength approximation ($\nu, \mu = (c, v)$). Here, Δ is the gap between the conduction and valence bands, v_F is the Fermi velocity, and $\theta_{\mathbf{k},\mathbf{q}}$ is the angle between the \mathbf{k} and \mathbf{q} wave vectors.

Energy dispersion		Overlap integral	
Standard	$\varepsilon_c(\mathbf{k}) = \frac{\hbar^2}{2m} k^2$; $\varepsilon_v(\mathbf{k}) = \Delta - \frac{\hbar^2}{2m} k^2$	$\mathcal{F}_{\nu,\mu}(\mathbf{k}, \mathbf{q}) = \delta_{\nu\mu} + (1 - \delta_{\nu\mu}) \frac{\hbar^2 q^2}{2m} \frac{\Delta}{(2\varepsilon_c(\mathbf{k}) + \Delta)^2}$	
Dirac	$\varepsilon_c(\mathbf{k}) = -\varepsilon_v(\mathbf{k}) = \hbar v_F k$	$\mathcal{F}_{\nu,\mu}(\mathbf{k}, \mathbf{q}) = \delta_{\nu\mu} + (1 - \delta_{\nu\mu}) \frac{\hbar^2 v_F^2 q^2}{4\varepsilon_c^2(\mathbf{k})} \sin^2 \theta_{\mathbf{k},\mathbf{q}}$	

conductivity tensor of 3D Weyl semimetals [20]. It is also important to note that in both types of 1D materials, the response is dominated by the intraband part as we have found that $\chi_{0,inter}^{(1)}(\mathbf{q}, \omega) \ll \chi_{0,intra}^{(1)}(\mathbf{q}, \omega)$ (see Supplementary Information). This implies that metallic-like response behavior is expected for 1D systems.

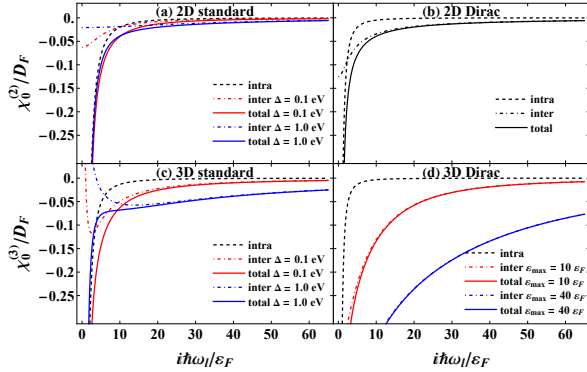


Figure 2. The intraband $\chi_{0,intra}^{(N)}$, interband $\chi_{0,inter}^{(N)}$, and total $\chi_0^{(N)} = \chi_{0,intra}^{(N)} + \chi_{0,inter}^{(N)}$ bare polarization versus imaginary frequency at $q = k_F$ are shown for various 2D, 3D standard materials (a,c) and for 2D, 3D gapless Dirac materials (b,d). For all Dirac materials $\varepsilon_F = 50$ meV, $g = 4$, $v_F = c/300$, while $g = 2$, $m = m_e$ for standard materials. The bare polarization function is scaled by the density of states at the Fermi level according to: $D_F^{(2),D} = \frac{g}{2\pi} \frac{\varepsilon_F}{\hbar^2 v_F^2}$, $D_F^{(3),D} = \frac{g}{2\pi^2} \frac{\varepsilon_F^2}{\hbar^3 v_F^3}$ for Dirac materials, $D_F^{(2),S} = \frac{g}{4\pi} \frac{2m}{\hbar^2}$ and $D_F^{(3),S} = \frac{g}{4\pi^2} \left(\frac{2m}{\hbar^2} \right)^{3/2} \varepsilon_F^{1/2}$ for standard materials.

At this stage, we examine the quantum mechanical limit of the vdW interaction from Eq. Equation (1) by substituting $\frac{2\pi k_B T}{\hbar} \sum_{l=0}^{+\infty}$ with integration over frequency $\int_0^\infty d\omega$ and taking the polarization function

in Eq. Equation (3) at $T = 0$. Asymptotic expressions for the vdW force can be found in the long wave approximation by also taking into account the Coulomb interactions in Table 1, the energy band structures in Table 2 for the considered materials, and their polarization functions in the Supplementary Information. The obtained expressions are organized in Table 3. We find that the force for both types of 1D systems for which $\varepsilon_F > 0$ is quite similar. In fact, the only difference is that $\hbar v_F$ for Dirac materials is replaced by $2\hbar^2 \varepsilon_F / m$ for standard materials, but the characteristic $[d\sqrt{\ln(2.2d/w)}]^{-3}$ scaling law is the same. The obtained distance dependence is consistent with previous results for different types of 1D materials [7, 21, 10]. This indicates that as long as $\varepsilon_F > 0$ the particular electronic structure plays a secondary effect in the interaction. For 1D parabolic materials with a finite gap, the interaction has a d^{-6} dependence indicating London type of behavior, which was also found for graphene nanoribbons [22]. The coupling in this case can further be tuned by changing the band gap since $F^{(1)S} \sim \Delta^{-2}$. We finally note that for 1D Dirac materials with $\varepsilon_F = 0$, $\chi_0^{(1)} \rightarrow 0$ in long wavelength limit, thus the vdW force is negligible.

The scaling laws in the vdW force at 2D are quite diverse. Dirac layers whose Fermi levels pass through the Dirac points interact with a force $F^{(2)D} \sim d^{-4}$. We note that a similar expression $F^{(2)D} = -\frac{3ge^2}{128\pi d^4}$ was obtained for two graphene layers in the retarded Casimir regime, where the Lifshitz formalism with accurate calculations of the optical response were used [23, 24, 25, 26, 27]. Such an expression was also found in other 2D Dirac materials by taking into account Hall conductivity response showing that topologically nontrivial features do not affect significantly the dispersive interaction at closer separations [28, 29, 27].

Table 3. Asymptotic scaling laws of the quantum mechanical and thermal vdW force of two identical Dirac and standard materials (degeneracy g) in 1D, 2D, and 3D. The dimensionless constants (analytical expressions given in the Supplementary Information) obtained from the calculations: $\mathcal{A}_{1S} \approx 0.01806$, $\mathcal{A}_{2S} \approx 0.01253$, $\mathcal{A}_{2D} \approx 0.007641$, $\mathcal{A}_{3S} \approx 0.438662$ and $\mathcal{A}'_{3S} \approx 2.12266$. For 3D Dirac materials, the numerical constant \mathcal{A}_{3D} depends on their Fermi velocity through the constant $\frac{ge^2}{\hbar v_F}$. Ex: $v_F = \frac{c}{300}$, $\mathcal{A}_{3D} \approx 0.397665$. The expressions for the thermal vdW force are the same for both types of materials.

	Dirac materials	Standard materials	Thermal limit
1D	$\frac{F^{(1)D}}{L} \rightarrow 0$ $\frac{F^{(1)D}}{L} = -\frac{1}{[d\sqrt{\ln(\frac{2.2d}{w})}]^3} \sqrt{\frac{ge^2 \hbar v_F}{32\pi^3}}$	$\frac{F^{(1)S}}{L} = -\frac{\mathcal{A}_{1S} g^2 e^4 \hbar^2}{m \Delta^2 d^6}$ $\frac{F^{(1)S}}{L} = -\frac{1}{[d\sqrt{\ln(\frac{2.2d}{w})}]^3} \sqrt{\frac{ge^2}{32\pi^3} \sqrt{\frac{2\varepsilon_F \hbar^2}{m}}}$	$\frac{F^{(1)T}}{L} = -\frac{\pi k_B T}{8[d\ln(\frac{6.3d}{w})]^2}$
2D	$\frac{F^{(2)D}}{A} = -\frac{\mathcal{A}_{2D} g e^2}{d^4}$ $\frac{F^{(2)D}}{A} = -\frac{\mathcal{A}_{2S} \sqrt{ge^2 \varepsilon_F / 2}}{d^{7/2}}$	$\frac{F^{(2)S}}{A} = -\frac{(1-\ln 2) g^2 e^4}{2\pi \Delta d^5}$ $\frac{F^{(2)S}}{A} = -\frac{\mathcal{A}_{2S} \sqrt{ge^2 \varepsilon_F}}{d^{7/2}}$	$\frac{F^{(2)T}}{A} = -\frac{\zeta(3) k_B T}{8\pi d^3}$
3D	$\frac{F^{(3)D}}{A} = -\frac{\mathcal{A}_{3D} \varepsilon_{max}}{8\pi^2 d^3}$	$\frac{F^{(3)S}}{A} = -\frac{\mathcal{A}_{3S}}{8\pi^2 d^3} \left(\frac{g^2 e^4 m}{\hbar^2}\right)^{1/3} \Delta^{2/3}$ $\frac{F^{(3)S}}{A} = -\frac{\mathcal{A}'_{3S}}{8\pi^2 d^3} \left(\frac{g^2 e^4 m}{\hbar^2}\right)^{1/4} \varepsilon_F^{3/4}$	$\frac{F^{(3)T}}{A} = -\frac{\zeta(3) k_B T}{8\pi d^3}$

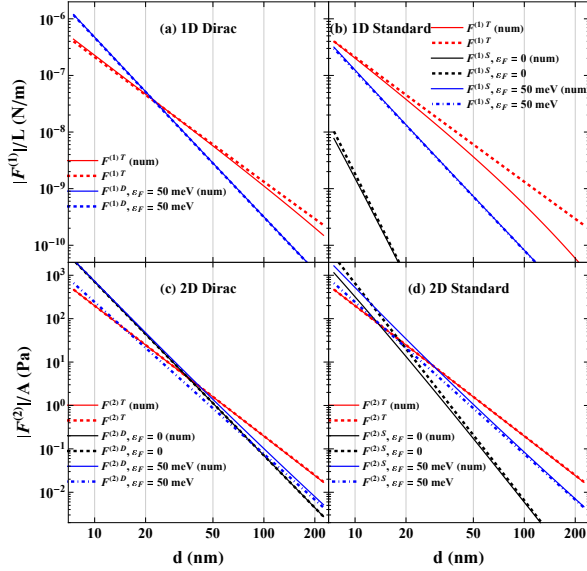


Figure 3. The vdW force per unit length (L) or unit area (A) in the quantum and thermal limits for (a) 1D Dirac materials, (b) 1D standard materials, (c) 2D Dirac materials and (d) 2D standard materials. Here $T = 300$ K, $\tau = 0.13$ ps, $\varepsilon_F = 50$ meV, $g = 4$, $v_F = c/300$ for Dirac materials and $g = 2$, $m = m_e$, $\Delta = 1$ eV for standard materials. The abbreviation (num) denotes calculations obtained by numerical evaluations of all quantities using Eqs. Equation (1), Equation (2) and Equation (3), while the rest of the data are found by the asymptotic scaling laws given in Table 3.

Actually, we find that the numerical constant $\mathcal{A}_{2D} = \frac{1}{16\pi} \int_0^{+\infty} \int_0^{+\infty} \frac{e^{-2u} u^2 du dv}{(1+vu)^2 - e^{-2u}} \approx 0.007641$ compares very well with $\frac{3}{128\pi}$. The difference of about 2% between the two results indicates that retardation and contributions from the transverse modes are not important in the dispersive interaction in such materials. One further notes that this interaction has the same scaling law as in perfect metals ($F_m =$

$-\frac{\hbar c \pi^2}{240 d^4}$), however the magnitude is much reduced (at least by two orders). Notably, the scaling law d^{-4} is consistent with any polarization function whose function dependence is $\chi_0^{(2)} \sim qf(\omega/q)$ as long as $\varepsilon_F = 0$ [9]. When $\varepsilon_F > 0$, the quantum vdW force for Dirac and standard materials displays $d^{-7/2}$ behavior. Such a scaling dependence is consistent with results found by others [6, 30, 31, 7, 32] when considering non-retarded dispersive interactions between different metals. The presence of an energy gap in the parabolic band structure changes the distance dependence to $F^{(2)D} \sim d^{-5}$ indicating a longer ranged interaction when comparing 2D metals and dielectrics [33, 7, 22].

For 3D systems, $F^{(3)} \sim d^{-3}$ for all cases showing a universal scaling law in the non-retarded regime. It is interesting to note that for Dirac materials, the explicit dependence of the polarization function upon ε_{max} specifying the validity of linear dispersion carries over to the vdW interaction as seen in the constant \mathcal{A}_{3D} (which in general depends on ε_{max} , see Supplementary Material). In fact, the $F^{(3)} \sim d^{-3}$ scaling functionality is also valid at larger separations when retardation is included and this is the case not only for Dirac materials, but also for Weyl semimetals whose 3D Dirac energy cones are non-degenerate [20, 34]. For standard systems, the quantum vdW force directly depends on the Fermi level in the case of metals or the band gap in the case of dielectrics.

Next we consider the thermal limit of the vdW interaction by examining the $l = 0$ term in Eq. Equation (1). For this purpose, the polarization function is calculated at finite temperature by utilizing the Maldague formula [35, 36],

$$\chi_0^{(N)}(\mathbf{q}, \omega_l, T > 0, \varepsilon_F, \tau) = \int_0^{+\infty} \frac{\chi_0^{(N)}(\mathbf{q}, \omega_l + \frac{1}{2\tau}, T = 0, \varepsilon'_F) d\varepsilon'_F}{4k_B T \cosh^2\left(\frac{\varepsilon_F - \varepsilon'_F}{2k_B T}\right)} \quad (4)$$

which also takes into account the relaxation time τ (assumed to be constant) due to scattering processes in the materials. The results from our calculations are given in Table 3. They indicate that the thermal vdW interaction is primarily determined by the dimensionality of the objects and the materials properties play a secondary role. For 1D systems $F^{(1)T} \sim [d \ln(6.5d/w)]^{-2}$, while the scaling law d^{-3} is the same for 2D and 3D interacting materials.

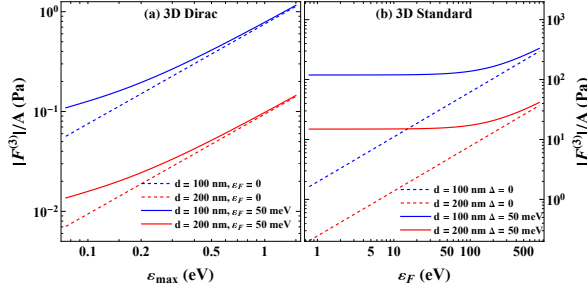


Figure 4. The vdW force per unit area (A) in 3D: (a) as a function of bandwidth ε_{max} for Dirac materials and (b) as a function of Fermi level ε_F for standard materials. Here $T = 300$ K, $\tau = 0.13$ ps, $\varepsilon_F = 50$ meV, $g = 4$, $v_F = c/300$ for Dirac materials and $g = 2$, $m = m_e$ for standard materials.

To gain further insight into the vdW interaction, the quantum mechanical and thermal forces are shown graphically as a function of distance in Fig. 3. For 1D Dirac materials (Fig. 3a), we find that the two limits coincide at $d_T \approx 20$ nm and at larger separations the magnitude of $F^{(1)T}$ becomes larger due to the slower distance decay compared to $F^{(1)D}$. For standard 1D interacting materials, the quantum vdW attraction is always smaller than the thermal limit in the range of interest 10 – 200 nm. In the case of 1D materials for which $\Delta \neq 0$, $F^{(1)D}$ falls very fast as the separation is increased, as can be seen in Fig. 3b indicating the dominance of thermal fluctuations.

For 2D materials, cross-over between different regimes is also observed. Particularly for 2D Dirac materials with $\varepsilon_F = 0$, the thermal force begins to dominate over the quantum limit for $d > d_T \approx 35$ nm, while this happens at $d > d_T \approx 40$ nm when $\varepsilon_F = 50$ meV for the two Dirac layers (Fig. 3c). Transitioning from a quantum mechanical to a thermal limit is also observed in Fig. 3d for standard materials, although the distance where that occurs is reduced. For example, the thermal force becomes larger at $d > d_T \approx 15$ nm for parabolic materials with $\varepsilon_F = 0$, while this effect is found for $d_T \approx 30$ nm for parabolic materials with $\varepsilon_F = 50$ meV.

For 3D materials, the vdW force is always $\sim d^{-3}$. For Dirac systems, the quantum force depends linearly on the bandwidth ε_{max} as shown in Fig. 4a. For standard materials, the interaction can be modulated by the Fermi level, as shown in Fig. 4b. As ε_F

lies inside a non-zero energy gap, the quantum vdW is completely determined by Δ at a given distance according to $F^{(3)S} \sim \Delta^{2/3}$. When $\Delta = 0$ or ε_F is in the conduction or valence region, $F^{(3)S} \sim \varepsilon_F^{3/4}$ as shown in Fig. 4b.

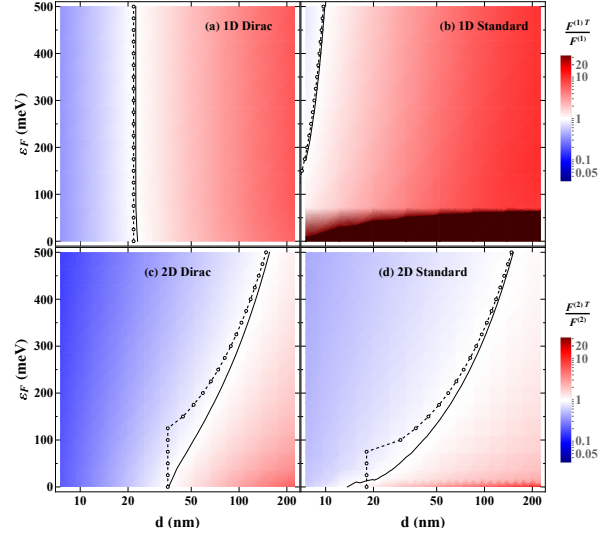


Figure 5. Density plots of the ratio $F^{(N)D,S}/F^{(N)T}$ between the quantum and thermal vdW force at $T = 300$ K in ε_F - d space. The solid black lines obtained numerically by using Equations (S-19), (S-21) and (S-23) in the Supplementary Material, and the dot-dashed lines obtained analytically by using the asymptotic scaling laws in Table 3, show when the limits coincide. Regions in blue correspond to the dominance of quantum mechanical effects, while regions in red correspond to dominating thermal effects, according to the given color bar. Here $\tau = 0.13$ ps, $g = 4$, $v_F = c/300$ for Dirac materials and $g = 2$, $m = m_e$, $\Delta = 1$ eV for standard materials.

A question of fundamental importance is how to better understand the characteristic distance d_T separating the quantum mechanical and thermal limits of the nonretarded vdW interaction involving different materials. Given the analytical expressions in Table 3, equating $F^{(N)D,S} = F^{(N)T}$ gives the means of finding d_T at which the quantum-to-thermal transition occurs. In Fig. 5, we show contour plots of $F^{(N)D,S}/F^{(N)T}$ in the ε_F vs d map, where d_T is clearly marked. It is interesting to note that in 1D materials (Fig. 5a,b), the thermal effects are especially strong. In systems with linear band dispersion, we find that $d_T = \frac{\sqrt{2}ge^2\hbar v_F}{\pi^{5/2}k_B T} \ln^2 \left(\frac{6.5\sqrt{2}ge^2\hbar v_F}{\pi^{5/2}wk_B T} \right) \ln^{-3/2} \left(\frac{2.2\sqrt{2}ge^2\hbar v_F}{\pi^{5/2}wk_B T} \right)$, which does not depend on the Fermi level ε_F . In standard materials, however, practically the entire region is dominated by thermal fluctuations. Separations smaller than 10 nm must be considered (which may involve taking into account the atomic structure of the materials) in order to have dominating quantum effects in the vdW interaction for 1D materials.

Significant thermal effects are also found in 2D

materials, as shown in Fig. 5c,d. We obtain that for small ε_F where $F^{(2)D} \sim 1/d^{-4}$, $d_T = \frac{8\pi A_{2D} q e^2}{\zeta(3) k_B T}$. For larger ε_F where $F^{(2)D} \sim 1/d^{-7/2}$, $d_T = \left(\frac{8\pi A_{2D}}{\zeta(3)}\right)^2 \frac{q e^2 \varepsilon_F}{k_B^2 T^2}$. These results show that in the first situation, d_T is independent of the Fermi level and it is $\sim T^{-1}$, while in the second situation $d_T \sim \varepsilon_F / (k_B T)^2$. In the case of 2D standard materials, for $F^{(2)S} \sim 1/d^{-5}$ corresponding to small Fermi levels, the characteristic thermal distance $d_T = \sqrt{\frac{4(1-\ln 2)}{\zeta(3)} \frac{q e^2}{\sqrt{k_B T \Delta}}} \sim T^{-1/2}$, while for $F^{(2)S} \sim 1/d^{-7/2}$ corresponding to large Fermi levels, $d_T = \left(\frac{8\pi A_{2D}}{\zeta(3)}\right)^2 \frac{q e^2 \varepsilon_F}{k_B^2 T^2} \sim \varepsilon_F / (k_B T)^2$.

For 3D materials, the quantum-to-thermal transition is controlled by other properties entering the expressions for the interaction, since the d^{-3} scaling law is the same for both limits. We find that $\frac{F^{(3)T}}{F^{(3)D}} \sim \frac{k_B T}{\varepsilon_{max}}$, which emphasizes again the importance of the bandwidth specifying the validity of the linear dispersion. For 3D parabolic materials, $\frac{F^{3T}}{F^{3S}} \sim \left(\frac{\hbar^2}{g^2 e^4 m}\right)^{1/4} \frac{k_B T}{\varepsilon_F^{3/4}}$ or $\frac{F^{(3)T}}{F^{(3)S}} \sim \left(\frac{\hbar^2}{g^2 e^4 m}\right)^{1/3} \frac{k_B T}{\Delta^{2/3}}$, which shows that the onset of thermal fluctuations can be controlled via the Fermi level or nonzero band gap in a similar way. To get an idea about the thermal characteristic distance in the non-retarded vdW regime, one must go beyond the long wavelength approximation and perhaps include retardation effects. This, however, may involve a different method of calculations, which goes beyond the scope of this paper.

3. Conclusions

In summary, the dispersive vdW interaction has been studied with the RPA method for materials with parabolic and linear energy dispersions. The quantum mechanical and thermal regimes are investigated in the case of interacting identical 1D, 2D, and 3D systems. We find that there is an intricate and potentially tunable by the Fermi level relationship between dimensionality and response properties relationship in the dispersive force.

The interaction between 1D materials is dominated by thermal fluctuations regardless of the energy band structure. In 2D materials, however, the characteristic distance for the quantum-to-thermal transitions depends strongly on the Fermi level with the general trend that larger ε_F results in larger d_T . By changing $\varepsilon_F = (0, 200)$ meV, $d_T \sim (35, 75)$ nm for Dirac and $d_T \sim (15, 70)$ nm for standard materials. Similar results for the onset of thermal effects can be found for the retarded Casimir interaction between undoped graphene layers for which $d_T = \hbar v_F / k_B T \sim 30$ nm [37, 38, 39, 40, 41]. Our calculations show that such

characteristic thermal distances are typical not only for Dirac materials, but also for standard parabolic systems in 2D. Comparing with the Casimir thermal distance for 3D metals $d_T = \hbar c / k_B T = 7.6 \times 10^3$ nm shows that thermal fluctuations become prominent at much smaller separations. It further appears that dimensionality is a leading factor in determining the onset of thermal effects, while the materials properties may be less important with the exception of 2D Dirac materials with $\varepsilon_F = 0$. In this case, regardless of ε_F , d_T for the non-retarded regime is always smaller by at least an order comparing with the micrometer d_T range that is typical for the retarded Casimir regime for 3D materials.

It is also interesting to note that the onset of thermal effects in the vdW regime in 3D is controlled by the ratio of $k_B T$ and various energy parameters ($\varepsilon_{max}, \varepsilon_F, \Delta$) of the materials, as discussed above. In all cases however, the thermal contribution becomes more prominent with temperature, but this effect can be modulated by other band structure properties. In the case of 3D Dirac materials, for example, $F^{3T} > F^{3D}$ occurs for $\varepsilon_{max} < 0.023$ eV at $T = 300$ K, since $\varepsilon_{max} < k_B T$. The explicit dependence upon ε_{max} is a direct consequence of the presence of the bandwidth in the polarization function. Since the scaling law for the interaction in 3D is the same regardless of the energy bands, we conclude that the onset of thermal effects can occur at any separation providing $k_B T$ is large enough or $\varepsilon_{max}, \varepsilon_F, \Delta$ parameters are small enough to ensure $F^{3T} > F^{3D}$.

This investigation gives a comprehensive understanding of the characteristic functionalities and asymptotics of vdW interactions at separations where retardation can be neglected. Our studies highlight the interplay between energy dispersion and dimensionality in the quantum mechanical and thermal limits of the vdW force. Interestingly, we find that thermal fluctuations for systems with reduced dimensions can become pronounced at much smaller separations when compared to their 3D counterparts. Our results provide a comprehensive picture of nonretarded dispersive interactions, which is complementary to previous in-depth studies focusing on the retarded Casimir regime [1, 2]. They can serve as a useful guidance to future experiments that might be geared towards demonstrating the pronounced role of thermal fluctuations at much reduced separations, a previously unexplored area.

4. Acknowledgments

L.M.W. acknowledges financial support from the US Department of Energy under grant No. DE-FG02-06ER46297. P. R.-L. was supported by "AYUDA PUENTE 2021, URJC".

- [1] Woods L M, Dalvit D A R, Tkatchenko A, Rodriguez-Lopez P, Rodriguez A W and Podgornik R 2016 *Rev. Mod. Phys.* **88**(4) 045003
- [2] Klimchitskaya G L, Mohideen U and Mostepanenko V M 2009 *Rev. Mod. Phys.* **81**(4) 1827–1885
- [3] Girifalco L A, Hodak M and Lee R S 2000 *Phys. Rev. B* **62**(19) 13104–13110
- [4] Ulbricht H, Moos G and Hertel T 2002 *Phys. Rev. B* **66**(7) 075404
- [5] Dobson J F 2014 *International Journal of Quantum Chemistry* **114** 1157–1161 ISSN 00207608
- [6] Sernelius B E and Björk P 1998 *Phys. Rev. B* **57**(11) 6592–6601
- [7] Dobson J F, White A and Rubio A 2006 *Physical Review Letters* **96** 073201 ISSN 0031-9007
- [8] Dobson J F, Gould T and Klich I 2009 *Physical Review A* **80** 012506 ISSN 1050-2947
- [9] Gómez-Santos G 2009 *Phys. Rev. B* **80**(24) 245424
- [10] Drosdoff D and Woods L M 2014 *Phys. Rev. Lett.* **112**(2) 025501
- [11] Dobson J F and Gould T 2012 *Journal of Physics: Condensed Matter* **24** 073201 ISSN 0953-8984
- [12] DiStasio R A, Gobre V V and Tkatchenko A 2014 *Journal of Physics: Condensed Matter* **26** 213202 ISSN 0953-8984
- [13] Liu P, Williams J R and Cha J J 2019 *Nature Reviews Materials* **4** 479–496 ISSN 2058-8437
- [14] Kumar N, Guin S N, Manna K, Shekhar C and Felser C 2021 *Chemical Reviews* **121** 2780–2815 ISSN 0009-2665
- [15] Fetter A L and Walecka J D 2003 *Quantum Theory of Many-Particle Systems* (Dover Publications) ISBN 0-486-42827-7
- [16] Hwang E H and Das Sarma S 2007 *Phys. Rev. B* **75**(20) 205418
- [17] Das Sarma S and Hwang E H 2009 *Phys. Rev. Lett.* **102**(20) 206412
- [18] Sachdeva R, Thakur A, Vignale G and Agarwal A 2015 *Phys. Rev. B* **91**(20) 205426
- [19] Ehrenreich H and Cohen M H 1959 *Phys. Rev.* **115**(4) 786–790
- [20] Rodriguez-Lopez P, Popescu A, Fialkovsky I, Khusnutdinov N and Woods L M 2020 *Communications Materials* **1** 14 ISSN 2662-4443
- [21] Drummond N D and Needs R J 2007 *Physical Review Letters* **99** 166401 ISSN 0031-9007
- [22] Stedman T, Drosdoff D and Woods L M 2014 *Physical Review A* **89** 012509 ISSN 1050-2947
- [23] Drosdoff D and Woods L M 2010 *Physical Review B - Condensed Matter and Materials Physics* **82** 155459 ISSN 10980121
- [24] Sarabadani J, Naji A, Asgari R and Podgornik R 2011 *Phys. Rev. B* **84**(15) 155407
- [25] Klimchitskaya G L, Mostepanenko V M and Sernelius B E 2014 *Phys. Rev. B* **89**(12) 125407
- [26] Klimchitskaya G L and Mostepanenko V M 2020 *Phys. Rev. D* **102**(1) 016006
- [27] Lu B S 2021 *Universe* **7** 237 ISSN 2218-1997
- [28] Rodriguez-Lopez P, Kort-Kamp W J M, Dalvit D A R and Woods L M 2017 *Nature Communications* **8** 14699 ISSN 2041-1723
- [29] Fialkovsky I, Khusnutdinov N and Vassilevich D 2018 *Phys. Rev. B* **97**(16) 165432
- [30] Dobson J F, McLennan K, Rubio A, Wang J, Gould T, Le H M and Dinte B P 2001 *Australian Journal of Chemistry* **54** 513 ISSN 0004-9425
- [31] Boström M and Sernelius B E 2000 *Phys. Rev. B* **61**(3) 2204–2210
- [32] Rodriguez-Lopez P and Grushin A G 2014 *Phys. Rev. Lett.* **112**(5) 056804
- [33] Rydberg H, Dion M, Jacobson N, Schröder E, Hyldgaard P, Simak S I, Langreth D C and Lundqvist B I 2003 *Phys. Rev. Lett.* **91**(12) 126402
- [34] Bordag M, Fialkovsky I, Khusnutdinov N and Vassilevich D 2021 *Phys. Rev. B* **104**(19) 195431
- [35] Maldague P F 1978 *Surface Science* **73** 296–302 ISSN 00396028
- [36] Ando T, Fowler A B and Stern F 1982 *Reviews of Modern Physics* **54** 437–672 ISSN 0034-6861
- [37] Khusnutdinov N, Kashapov R and Woods L M 2018 *2D Materials* **5** 035032 ISSN 2053-1583
- [38] Drosdoff D, Phan A D, Woods L M, Bondarev I V and Dobson J F 2012 *The European Physical Journal B* **85** 365 ISSN 1434-6028
- [39] Liu M, Zhang Y, Klimchitskaya G L, Mostepanenko V M and Mohideen U 2021 *Phys. Rev. B* **104**(8) 085436
- [40] Bimonte G, Klimchitskaya G L and Mostepanenko V M 2017 *Phys. Rev. B* **96**(11) 115430
- [41] Klimchitskaya G L and Mostepanenko V M 2015 *Phys. Rev. B* **91**(17) 174501

Supplementary Information for Dispersive interaction between standard and Dirac materials: dispersion and dimensionality effects

Dai-Nam Le,^{1,2,3,*} Pablo Rodriguez-Lopez,^{4,†} and Lilia M. Woods^{1,‡}

¹*Department of Physics, University of South Florida, Tampa, Florida 33620, USA*

²*Atomic Molecular and Optical Physics Research Group, Advanced Institute of Materials Science,
Ton Duc Thang University, Ho Chi Minh City 700000, Vietnam*

³*Faculty of Applied Sciences, Ton Duc Thang University, Ho Chi Minh City 700000, Vietnam*

⁴*Área de Electromagnetismo and Grupo Interdisciplinar de Sistemas Complejos (GISC),
Universidad Rey Juan Carlos, 28933, Móstoles, Madrid, Spain*

(Dated: February 3, 2022)

S-I. THE COULOMB INTERACTION

The Coulomb interaction between two objects separated by a distance d along the z axis in reciprocal \mathbf{q} space is found by using Fourier transformation in standard electrostatics,

$$\mathcal{V}^{(N)}(\mathbf{q}, d) = \int U_c(\mathbf{r}, d) e^{i\mathbf{q}\cdot\mathbf{r}} d^N \mathbf{r} = e^2 \int \frac{1}{\kappa \sqrt{r_\perp^2 + (r_\parallel + d)^2}} e^{i\mathbf{q}\cdot\mathbf{r}} d^N \mathbf{r}. \quad (\text{S-1})$$

Note that in 1D $r_\perp = x, r_\parallel = 0$, in 2D $r_\perp = \sqrt{x^2 + y^2}, r_\parallel = 0$, and in 3D $r_\perp = \sqrt{x^2 + y^2}, r_\parallel = z$. After performing the integral (S-1), the result is given as follows:

$$\mathcal{V}^{(N)}(\mathbf{q}, d) = \begin{cases} 2e^2 K_0(|q|d) & N = 1 \\ (2\sqrt{\pi})^{N-1} \Gamma\left(\frac{N-1}{2}\right) \frac{e^2}{q^{N-1}} e^{-q_\perp d} & N = 2, 3 \end{cases} \quad (\text{S-2})$$

The Coulomb interaction inside each material corresponds to $v_0^{(N)}(q) = \lim_{d \rightarrow 0} \mathcal{V}^{(N)}(\mathbf{q}, d)$, such that

$$v_0^{(N)}(\mathbf{q}) = \begin{cases} 2e^2 \left[\ln\left(\frac{2}{|q|w}\right) - \gamma_E \right] & N = 1 \\ (2\sqrt{\pi})^{N-1} \Gamma\left(\frac{N-1}{2}\right) \frac{e^2}{q^{N-1}} & N = 2, 3. \end{cases} \quad (\text{S-3})$$

S-II. POLARIZATION FUNCTION FOR STANDARD AND DIRAC MATERIALS IN THE LONG-WAVELENGTH LIMIT

The bare polarization $\chi_0^{(N)}(\mathbf{q}, \omega)$ consists of intraband and interband components, given as

$$\chi_{0,intra}^{(N)}(\mathbf{q}, \omega) = \int \frac{gd^N \mathbf{k}}{(2\pi)^N} \left[\mathcal{F}_{c,c}(\mathbf{k}, \mathbf{q}) \frac{f(\varepsilon_c(\mathbf{k})) - f(\varepsilon_c(\mathbf{k} + \mathbf{q}))}{i\hbar\omega - [\varepsilon_c(\mathbf{k} + \mathbf{q}) - \varepsilon_c(\mathbf{k})]} + \mathcal{F}_{v,v}(\mathbf{k}, \mathbf{q}) \frac{f(\varepsilon_v(\mathbf{k})) - f(\varepsilon_v(\mathbf{k} + \mathbf{q}))}{i\hbar\omega - [\varepsilon_v(\mathbf{k} + \mathbf{q}) - \varepsilon_v(\mathbf{k})]} \right], \quad (\text{S-4a})$$

$$\chi_{0,inter}^{(N)}(\mathbf{q}, \omega) = \int \frac{gd^N \mathbf{k}}{(2\pi)^N} \mathcal{F}_{c,v}(\mathbf{k}, \mathbf{q}) \left[\frac{f(\varepsilon_c(\mathbf{k})) - f(\varepsilon_v(\mathbf{k} + \mathbf{q}))}{i\hbar\omega - [\varepsilon_v(\mathbf{k} + \mathbf{q}) - \varepsilon_c(\mathbf{k})]} + \frac{f(\varepsilon_v(\mathbf{k})) - f(\varepsilon_c(\mathbf{k} + \mathbf{q}))}{i\hbar\omega - [\varepsilon_c(\mathbf{k} + \mathbf{q}) - \varepsilon_v(\mathbf{k})]} \right]. \quad (\text{S-4b})$$

* ledainam@tdtu.edu.vn

† pablo.ropez@urjc.es

‡ lmwoods@usf.edu; Author to whom all correspondence should be addressed

S-2

At $T = 0$ K, the Fermi-Dirac distribution $f(\varepsilon)$ becomes the Heaviside function $f(\varepsilon_\mu(\mathbf{k}, s)) \rightarrow \Theta(\varepsilon_F - \varepsilon_\mu(\mathbf{k}, s)) = \Theta(k_F - k)$. Here, $\Theta(x)$ and k_F denote the Heaviside step function and the Fermi momentum, respectively. By using the long wavelength approximation $q \rightarrow 0$ and keeping the lowest terms, we find

$$f(\varepsilon_c(\mathbf{k}, s)) - f(\varepsilon_c(\mathbf{k} + \mathbf{q}, s)) \approx \delta(k_F - k) q \cos \theta \quad (\text{S-5a})$$

$$f(\varepsilon_v(\mathbf{k}, s)) - f(\varepsilon_v(\mathbf{k} + \mathbf{q}, s)) \approx 0 \quad (\text{S-5b})$$

$$f(\varepsilon_c(\mathbf{k}, s)) - f(\varepsilon_v(\mathbf{k} + \mathbf{q}, s)) \approx -\Theta(k - k_F) \quad (\text{S-5c})$$

$$f(\varepsilon_v(\mathbf{k}, s)) - f(\varepsilon_c(\mathbf{k} + \mathbf{q}, s)) \approx +\Theta(k - k_F). \quad (\text{S-5d})$$

In the above expressions, θ is the angle between \mathbf{q} and \mathbf{k} wave vectors. One notes that these hold for both, standard and Dirac materials.

Again, with the lowest terms in the $q \rightarrow 0$ the overlap integral $\mathcal{F}_{\nu,\mu}(\mathbf{k}, \mathbf{q})$ is found as [1]

$$\mathcal{F}_{\nu,\mu}(\mathbf{k}, \mathbf{q}) \approx \delta_{\nu\mu} + (1 - \delta_{\nu\mu}) \left(\frac{q \mathcal{P}_{c,v}(k, \theta)}{\varepsilon_c(\mathbf{k}) - \varepsilon_v(\mathbf{k})} \right)^2 \quad (\text{S-6})$$

where $\mathcal{P}_{c,v}(k, \theta) = \left| \langle u_{c,\mathbf{k}} | \mathbf{e}_{\mathbf{q}} \cdot \partial_{\mathbf{k}} \hat{\mathcal{H}}_{\mathbf{k}} | u_{v,\mathbf{k}} \rangle \right| \approx \mathcal{P}_{c,v}(\theta)$. For all materials with parabolic dispersion, we find that $\mathcal{P}_{c,v}(k, \theta) = 0$.

Inserting approximations (S-5), (S-6) as well as the band structure and overlap form factor given in Table II into (S-4), we can obtain the zero-temperature of intraband and interband free polarization in the lowest term of q for both Dirac materials and standard materials. In Table S-I, the results for Dirac materials are given.

TABLE S-I. Intraband and interband components of the zero-temperature bare polarization function of Dirac materials in imaginary frequency.

	$\chi_{0,intra}^{(N)}(\mathbf{q}, i\omega)$	$\chi_{0,inter}^{(N)}(\mathbf{q}, i\omega)$
1D	$\chi_{0,intra}^{(1)D}(\mathbf{q}, i\omega) \approx -\frac{g}{\pi} \frac{q^2}{\hbar v_F \hbar^2 \omega^2}$	$\chi_{0,inter}^{(1)D}(\mathbf{q}, i\omega) \ll \chi_{0,intra}^{(1)D}(\mathbf{q}, i\omega)$
2D	$\chi_{0,intra}^{(2)D}(\mathbf{q}, i\omega) \approx -\frac{g}{4\pi} \frac{q^2 \varepsilon_F}{\hbar^2 \omega^2}$	$\chi_{0,inter}^{(2)D}(\mathbf{q}, i\omega) \approx -\frac{g}{8\pi} \frac{q^2}{\hbar \omega} \arctan\left(\frac{\hbar \omega}{2\varepsilon_F}\right)$
3D	$\chi_{0,intra}^{(3)D}(\mathbf{q}, i\omega) \approx -\frac{g}{6\pi^2} \frac{q^2}{\hbar v_F} \frac{\varepsilon_F^2}{\hbar^2 \omega^2}$	$\chi_{0,inter}^{(3)D}(\mathbf{q}, i\omega) \approx -\frac{g}{24\pi^2} \frac{q^2}{\hbar v_F} \ln\left(\frac{\hbar^2 \omega^2 + 4\varepsilon_{max}^2}{\hbar^2 \omega^2 + 4\varepsilon_F^2}\right)$

For 1D Dirac material, the leading term of interband polarization is of order $\frac{q^4}{(\hbar \omega)^4}$, thus it is much smaller than the intraband part meaning that the 1D massless Dirac material acts like a metal.

For 2D massless Dirac material for which $\varepsilon_F \ll \hbar \omega$, the second term in $\chi_{0,inter}^{(2)D}(\mathbf{q}, i\omega) \approx -\frac{g}{16} \frac{q^2}{\hbar \omega} + \frac{g}{4\pi} \frac{q^2 \varepsilon_F}{\hbar^2 \omega^2}$ cancels with the intraband polarization leading to total $\chi_0^{(2)D}(\mathbf{q}, i\omega) \approx -\frac{g}{16} \frac{q^2}{\hbar \omega}$, as already found by several authors [2–5] considering graphene and its optical conductivity $\sigma_0^{(2)D}(\mathbf{q}, i\omega) = \frac{-\omega e^2}{q^2} \chi_0^{(2)D}(\mathbf{q}, i\omega) = \frac{g e^2}{16 \hbar}$. The interband polarization in 3D Dirac materials depends explicitly on the bandwidth ε_{max} , as also noted by others [6].

The results for the intra and interband components of the polarization function are also summarized in Table S-II.

S-3

TABLE S-II. Intraband and interband components of the zero-temperature bare polarization function of standard materials in imaginary frequency. Here $f_+(\omega, \varepsilon_F) = \sqrt{\frac{1 + \frac{\hbar^2 \omega^2}{\Delta^2} + 1}{2}} \arccos\left(\frac{\frac{2\varepsilon_F}{\Delta} - \sqrt{1 + \frac{\hbar^2 \omega^2}{\Delta^2}}}{\sqrt{(1 + \frac{2\varepsilon_F}{\Delta})^2 + \frac{\hbar^2 \omega^2}{\Delta^2}}}\right)$ and $f_-(\omega, \varepsilon_F) = \sqrt{\frac{1 + \frac{\hbar^2 \omega^2}{\Delta^2} - 1}{2}} \operatorname{arccosh}\left(\frac{\frac{2\varepsilon_F}{\Delta} + \sqrt{1 + \frac{\hbar^2 \omega^2}{\Delta^2}}}{\sqrt{(1 + \frac{2\varepsilon_F}{\Delta})^2 + \frac{\hbar^2 \omega^2}{\Delta^2}}}\right)$.

	$\chi_{0,intra}^N(\mathbf{q}, i\omega)$	$\chi_{0,inter}^N(\mathbf{q}, i\omega)$
1D	$\chi_{0,intra}^{(1)S}(\mathbf{q}, i\omega) \approx -\frac{g}{\pi} \sqrt{\frac{2\hbar^2 \varepsilon_F}{m}} \frac{q^2}{\hbar^2 \omega^2}$	$\chi_{0,inter}^{(1)S}(\mathbf{q}, i\omega) \approx -\frac{g}{\pi} \sqrt{\frac{\hbar^2 \Delta}{m}} \frac{q^2}{\hbar^2 \omega^2} \left(\arctan \sqrt{\frac{\Delta}{2\varepsilon_F}} - \frac{f_+(\omega, \varepsilon_F) + f_-(\omega, \varepsilon_F)}{2\sqrt{1 + \frac{\hbar^2 \omega^2}{\Delta^2}}} \right)$
2D	$\chi_{0,intra}^{(2)S}(\mathbf{q}, i\omega) \approx -\frac{g}{4\pi} \frac{2q^2 \varepsilon_F}{\hbar^2 \omega^2}$	$\chi_{0,inter}^{(2)S}(\mathbf{q}, i\omega) \approx -\frac{g}{8\pi} \frac{q^2 \Delta}{\hbar^2 \omega^2} \ln\left(1 + \frac{\hbar^2 \omega^2}{(2\varepsilon_F + \Delta)^2}\right)$
3D	$\chi_{0,intra}^{(3)S}(\mathbf{q}, i\omega) \approx -\frac{g}{6\pi^2} \frac{\sqrt{2m\varepsilon_F}}{\hbar} \frac{2q^2 \varepsilon_F}{\hbar^2 \omega^2}$	$\chi_{0,inter}^{(3)S}(\mathbf{q}, i\omega) \approx \frac{g}{8\pi^2} \frac{\sqrt{m\Delta}}{\hbar} \frac{q^2 \Delta}{\hbar^2 \omega^2} \left(\arctan \sqrt{\frac{\Delta}{2\varepsilon_F}} - f_+(\omega, \varepsilon_F) + f_-(\omega, \varepsilon_F) \right)$

S-III. THE VDW FORCE BETWEEN DIRAC AND STANDARD MATERIALS

The quantum mechanical limit at $T = 0$ for the force is given below for the different cases. All expression are obtained by using that $\frac{2\pi k_B T}{\hbar} \sum_{l=-\infty}^{l=+\infty} \rightarrow \int_0^{+\infty} d\omega$. For 1D materials, one finds that

$$\frac{F^{(1)}}{L} = -\frac{\hbar}{\pi^2 d^2} \int_0^{+\infty} \int_0^{+\infty} \frac{K_1(\tilde{q}) \tilde{q} d \tilde{q} d\omega}{K_0(\tilde{q}) \left\{ \left[1 + \frac{\ln\left(\frac{d}{w}\right)}{K_0(\tilde{q})} + \left(\frac{d}{d_c^{(1)}(i\omega)}\right)^2 \frac{1}{\tilde{q}^2 K_0(\tilde{q})} \right]^2 - 1 \right\}}, \quad (\text{S-7})$$

where $\tilde{\mathbf{q}} = \mathbf{q}d$ and $d_c^{(1)}(i\omega) = \sqrt{-\frac{2e^2}{\tilde{q}^2} \chi_0^{(1)}\left(\frac{\tilde{\mathbf{q}}}{d}, i\omega\right)}$. In the long wavelength approximation, the formula (S-7) reads as

$$\frac{F^{(1)D}}{L} = \begin{cases} 0 & \varepsilon_F = 0 \\ -\frac{1}{[d\sqrt{\ln(\frac{d}{w})}]^3} \sqrt{\frac{ge^2 \hbar v_F}{32\pi^3}} & \varepsilon_F > 0 \end{cases}, \quad (\text{S-8})$$

while in the case of 1D standard materials, it becomes

$$\frac{F^{(1)S}}{L} = \begin{cases} -\frac{\mathcal{A}_{1S} g^2 e^4 \hbar^2}{m \Delta^2 d^6} & \frac{m \varepsilon_F^4 d^4}{g^2 e^4 \hbar^2 \Delta} \ll 1 \\ -\frac{1}{[d\sqrt{\ln(\frac{d}{w})}]^3} \sqrt{\frac{ge^2}{32\pi^3}} \sqrt{\frac{2\varepsilon_F \hbar^2}{m}} & \frac{m \varepsilon_F^4 d^4}{g^2 e^4 \hbar^2 \Delta} \gg 1 \end{cases}, \quad (\text{S-9})$$

where $\mathcal{A}_{1S} = \frac{135}{1024} \left(\frac{1}{3} - \frac{\pi}{16}\right) \approx 0.01806$. Here the numerical constant $\eta = \exp\left[2 \int_0^{+\infty} x^2 K_1(x) K_0^2(x) dx\right] \approx 2.2$ comes from the long-wavelength approximation of the integration.

For 2D materials, one writes

$$\frac{F^{(2)}}{A} = -\frac{\hbar}{2\pi^2 d^3} \int_0^{+\infty} \int_0^{+\infty} \frac{\tilde{q}^2 d \tilde{q} d\omega}{e^{2\tilde{q}} \left[1 + \frac{d}{d_c^{(2)}(i\omega)} \right]^2 - 1}, \quad (\text{S-10})$$

where $\tilde{\mathbf{q}} = \mathbf{q}d$ and $d_c^{(2)}(i\omega) = -\frac{2\pi e^2}{\tilde{q}^2} \chi_0^{(2)}\left(\frac{\tilde{\mathbf{q}}}{d}, i\omega\right)$. In the case of 2D Dirac materials, (S-10) gives us the scaling laws of

$$\frac{F^{(2)D}}{A} = \begin{cases} -\frac{\mathcal{A}_{2D} g e^2}{d^4} & \frac{\varepsilon_F d}{g e^2} \ll 1 \\ -\frac{\mathcal{A}_{2S} \sqrt{g e^2 \varepsilon_F / 2}}{d^{7/2}} & \frac{\varepsilon_F d}{g e^2} \gg 1 \end{cases}, \quad (\text{S-11})$$

S-4

where $\mathcal{A}_{2D} = \frac{1}{16\pi} \left(6 \ln 2 - \frac{3\zeta(3)}{4} - \frac{\pi^2}{4} - \frac{\pi^4}{240} \right) \approx 0.007641$ and $\mathcal{A}_{2S} = \frac{1}{8\pi} \int_0^{+\infty} \frac{e^{-5\bar{q}/4} \bar{q}^{5/2} d\bar{q}}{\sqrt{2 \sinh \bar{q}} (\sqrt{\sinh \frac{\bar{q}}{2}} + \sqrt{\cosh \frac{\bar{q}}{2}})} \approx 0.01253$. In the case of 2D standard materials, the scaling laws obtained from (S-10) is given as

$$\frac{F^{(2)S}}{A} = \begin{cases} -\frac{(1-\ln 2)g^2 e^4}{2\pi \Delta d^6} \frac{\varepsilon_F d}{g e^2} \ll 1 \ll \frac{\Delta d}{g e^2} \\ -\frac{\mathcal{A}_{2S} \sqrt{g e^2 \varepsilon_F}}{d^{7/2}} \frac{\varepsilon_F d}{g e^2} \gg 1 \end{cases}. \quad (\text{S-12})$$

For 3D materials, we obtain

$$\begin{aligned} \frac{F^{(3)}}{A} &= -\frac{\hbar}{2\pi^2} \int_0^{q_{max}} \int_0^{\omega_{max}} \frac{q_{\perp}^2 dq_{\perp} d\omega}{e^{2q_{\perp} d} \left[1 - \frac{1}{4\pi e^2} \chi_0^{(3)}(q, \omega) \right]^2 - 1} \\ &= -\frac{1}{8\pi^2 d^3} \int_0^{+\infty} Li_3 \left[\left(\frac{\alpha(\varepsilon/\hbar)}{\alpha(\varepsilon/\hbar) + 1} \right)^2 \right] d\varepsilon \end{aligned} \quad (\text{S-13})$$

where $\varepsilon_{max} = \hbar\omega_{max} = \hbar v_F q_{max}$ for 3D Dirac materials and $\varepsilon_{max} = \hbar\omega_{max} = \hbar^2 q_{max}^2 / 2m$ for 3D standard materials, while $Li_3(z)$ is the 3th order polylogarithm function [7]. The integral $\int_0^{+\infty} Li_3 \left[\left(\frac{\alpha(\varepsilon/\hbar)}{\alpha(\varepsilon/\hbar) + 1} \right)^2 \right] d\varepsilon$ helps us find how the vdW force depends on the energy dispersion of the 3D materials. For gapped 3D standard materials, $\Delta > 0$, this integral approximately equals to

$$\int_0^{+\infty} Li_3 \left[\left(\frac{\alpha(\varepsilon/\hbar)}{\alpha(\varepsilon/\hbar) + 1} \right)^2 \right] d\varepsilon \approx \mathcal{A}_{3S} \left(\frac{g^2 e^4 m}{\hbar^2} \right)^{1/3} \Delta^{2/3}, \quad (\text{S-14})$$

where $\mathcal{A}_{3S} = \int_0^{+\infty} Li_3 \left(\frac{1}{(1+t^{3/2})^2} \right) dt \approx 0.438662$. In the case of 3D standard metal, $\varepsilon_F > 0$ and $\Delta = 0$, we have

$$\int_0^{+\infty} Li_3 \left[\left(\frac{\alpha(\varepsilon/\hbar)}{\alpha(\varepsilon/\hbar) + 1} \right)^2 \right] d\varepsilon \approx \mathcal{A}'_{3S} \left(\frac{g^2 e^4 m}{\hbar^2} \right)^{1/4} \varepsilon_F^{3/4}, \quad (\text{S-15})$$

where $\mathcal{A}'_{3S} = \sqrt[4]{\frac{32\pi^2}{9}} \int_0^{+\infty} Li_3 \left(\frac{1}{(1+t^2)^2} \right) dt \approx 2.12266$. In the case of 3D Dirac materials, the polarizability is

$$\alpha^{(3)D} \left(\frac{\varepsilon}{\hbar} \right) = \frac{g e^2}{6\pi \hbar v_F} \left[\frac{4\varepsilon_F^2}{\varepsilon^2} + \ln \left(\frac{\varepsilon^2 + 4\varepsilon_{max}^2}{\varepsilon^2 + 4\varepsilon_F^2} \right) \right], \quad (\text{S-16})$$

which depends explicitly on the bandwidth ε_{max} . Thus the integral in (S-13) is obtained as

$$\int_0^{\varepsilon_{max}} Li_3 \left[\left(\frac{\alpha(\varepsilon/\hbar)}{\alpha(\varepsilon/\hbar) + 1} \right)^2 \right] d\varepsilon = \mathcal{A}_{3D} \varepsilon_{max}, \quad (\text{S-17})$$

where

$$\begin{aligned} \mathcal{A}_{3D} &= \int_{\ln 4}^{+\infty} Li_3 \left(\frac{\left(t + \frac{\varepsilon_F^2}{\varepsilon_{max}^2} (e^t - 1) - \ln \left(1 + \frac{\varepsilon_F^2}{\varepsilon_{max}^2} (e^t - 1) \right) \right)^2}{\left(t + \frac{\varepsilon_F^2}{\varepsilon_{max}^2} (e^t - 1) - \ln \left(1 + \frac{\varepsilon_F^2}{\varepsilon_{max}^2} (e^t - 1) \right) + \frac{6\pi \hbar v_F}{g e^2} \right)^2} \right) \frac{e^t}{(e^t - 1)^{3/2}} dt \\ &\approx \int_{\ln 4}^{+\infty} Li_3 \left(\frac{t^2}{\left(t + \frac{6\pi \hbar v_F}{g e^2} \right)^2} \right) \frac{e^t}{(e^t - 1)^{3/2}} dt, \end{aligned} \quad (\text{S-18})$$

for $\varepsilon_F \ll \varepsilon_{max}$. The numerical constant \mathcal{A}_{3D} depends on the dimensionless constant $\frac{g e^2}{6\pi \hbar v_F}$. For $g = 4$ and $v_F = \frac{c}{300}$, $\mathcal{A}_{3D} \approx 0.397665$.

The thermal limit of the vdW interaction is obtained by taking the $l = 0$ Matsubara frequency together with the Maldague formula for the polarization function, as given in the main text.

S-5

For 1D materials, one finds that

$$\frac{F^{(1)T}}{L} = -\frac{k_B T}{\pi d^2} \int_0^{+\infty} \frac{\tilde{q} K_1(\tilde{q}) d\tilde{q}}{K_0(\tilde{q}) \left\{ \left[1 + \frac{\ln(d/w)}{K_0(\tilde{q})} + \left(\frac{d}{d_c^{(1)}} \right)^2 \frac{1}{\tilde{q}^2 K_0(\tilde{q})} \right]^2 - 1 \right\}}, \quad (\text{S-19})$$

where $d_c^{(1)} = \sqrt{-\frac{2e^2}{q^2} \chi_0^{(1)} \left(\frac{\tilde{q}}{d}, 0, T, \varepsilon_F, \tau \right)}$. By taking $\tau \rightarrow +\infty \Rightarrow d_c^{(1)} \rightarrow +\infty$ and $d \ll d_c^{(1)}$, we find that

$$\frac{F^{(1)T}}{L} \rightarrow -\frac{\pi k_B T}{8 [d \ln(\eta_T d/w)]^2}, \quad (\text{S-20})$$

where the numerical constant $\eta_T = \exp \left[\frac{8}{\pi^2} \int_0^{+\infty} x^2 K_1(x) K_0^2(x) dx \right] \approx 6.5$, as found from the long wavelength approximation of the integration.

For 2D materials, one obtains

$$\frac{F^{(2)T}}{A} = -\frac{k_B T}{2\pi d^3} \int_0^{+\infty} \frac{\tilde{q}^2 d\tilde{q}}{e^{2\tilde{q}} \left[1 + \frac{d}{d_c^{(2)}} \right]^2 - 1}, \quad (\text{S-21})$$

where $d_c^{(2)} = -\frac{2\pi e^2}{q^2} \chi_0^{(2)} \left(\frac{\tilde{q}}{d}, 0, T, \varepsilon_F, \tau \right)$. Again, by taking $\tau \rightarrow +\infty \Rightarrow d_c^{(2)} \rightarrow +\infty$ and $d \ll d_c^{(2)}$, we find that

$$\frac{F^{(2)T}}{A} \rightarrow -\frac{\zeta(3) k_B T}{8\pi d^3}, \quad (\text{S-22})$$

For 3D materials, one obtains

$$\frac{F^{(3)T}}{A} = -\frac{k_B T}{8\pi d^3} Li_3 \left[\left(\frac{\alpha(\frac{1}{2\tau}, T, \varepsilon_F)}{\alpha(\frac{1}{2\tau}, T, \varepsilon_F) + 1} \right)^2 \right]. \quad (\text{S-23})$$

By taking $\tau \rightarrow +\infty$, one finds that

$$\frac{F^{(3)T}}{A} \rightarrow -\frac{\zeta(3) k_B T}{8\pi d^3}. \quad (\text{S-24})$$

-
- [1] H. Ehrenreich and M. H. Cohen, *Phys. Rev.* **115**, 786 (1959).
 - [2] K. W. K. Shung, *Phys. Rev. B* **34**, 979 (1986).
 - [3] J. González, F. Guinea, and M. Vozmediano, *Nuclear Physics B* **424**, 595 (1994).
 - [4] G. Gómez-Santos, *Phys. Rev. B* **80**, 245424 (2009).
 - [5] E. H. Hwang and S. Das Sarma, *Phys. Rev. B* **75**, 205418 (2007).
 - [6] P. Rodríguez-Lopez, A. Popescu, I. Fialkovsky, N. Khusnutdinov, and L. M. Woods, *Communications Materials* **1**, 14 (2020).
 - [7] A. A. Abrikosov, L. P. Gorkov, and I. E. Dzyaloshinski, *Methods of Quantum field theory in Statistical Physics* (Dover Publications, 1975).